Evaluating the Performance of Single and Double Moment Microphysics Schemes During a Synoptic-Scale Snowfall Event

Andrew L. Molthan

NASA Short-term Prediction Research and Transition (SPoRT) Center, Marshall Space Flight Center, Huntsville, AL

1. Introduction

Increases in computing power have lead to the experimental or operational use of high resolution weather forecast models that attempt to explicitly resolve precipitation processes by using bulk-water microphysics schemes capable of predicting both the mass content and size distribution of several hydrometeor species. These approaches have been used to predict the convective mode for severe weather events (Kain et al. 2006) and the development of mesoscale snow bands responsible for heavy snowfall (Bernardet et al. 2008).

Several bulk water microphysics schemes are available within the Weather Research and Forecasting (WRF) model as of version 3.1.1, with varying numbers of simulated hydrometeor classes and methods for estimating their size distributions, densities, and fall speeds. In order to evaluate these various assumptions, field campaign data are necessary, providing measurement of particle size distributions, ice or liquid water content, inference of particle bulk densities, and their terminal fall speeds. Toward this goal, the Canadian CloudSat/CALIPSO Validation Project (C3VP) sought to obtain in situ observations of ice crystals and aggregates in order to evaluate various microphysics schemes, and to serve as a basis for evaluating satellite retrievals of cloud properties from current sensors and future members of the NASA Global Precipitation Measurement (GPM) mission. Centered in southern Ontario and managed at the Canadian Centre for Atmospheric Research Experiments (CARE), the C3VP campaign provided aircraft and surface measurements of ice crystals, dual-polarimetric radar data, and traditional surface weather observations during a synoptic-scale snowfall event on 22 January 2007. Herein, discussion focuses on the evaluation of WRF model forecasts for the 22 January 2007 event, utilizing aircraft and surface observations to evaluate the assumptions and overall performance of several bulk water microphysics schemes currently available to the operational forecasting community.

2. Characteristics of Single and Double Moment Bulk Water Microphysics Schemes

Single- and double-moment schemes vary by particle size distribution function, methods of calculating distribution shape parameters, relationships between mass and diameter, relationships between diameter and terminal fall speed, and a variety of assumptions within simulated microphysical processes. With the exception of the Thompson scheme, all single- or double-moment microphysics scheme used in this study use a form of the gamma distribution:

$$N_x(D) = N_{ox} D^{\mu_x} e^{-\lambda_x D}, \tag{1}$$

where N_{ox} is referred to as the size distribution intercept, μ_x is the dispersion parameter, and λ_x is the slope parameter. In the following analyses, the subscript x is replaced with 's' to denote references to the snow category. Marshall and Palmer (1948) determined that populations of large, precipitating ice crystals could be represented as an exponential size distribution, a special case of the gamma distribution (1) where μ_s is set to zero:

$$N_s(D) = N_{os} e^{-\lambda_s D} \tag{2}$$

The total mass content within the size distribution can be determined by integrating the product of (1) or (2) and a mass-diameter relationship. Locatelli and Hobbs (1974) determined mass-diameter, or $M(D)$ relationships for several types of crystals in a power-law form:

$$M(D) = a_m D^{b_m} \tag{3}$$

Locatelli and Hobbs (1974) observed that the coefficient a_m varied by crystal type and degree of riming, while the exponent values of b_m averaged near 2 and suggested that the mass of a crystal was proportional to cross-sectional area. If crystals are represented by an equivalent diameter sphere with an effective density of ρ_s, then the coefficient $a_m = \frac{\pi}{6}\rho_s$ and exponent $b_m = 3$. By combining (2) and (3), and integrating over the entire size distribution the total mass content can be determined:

$$M = \int_0^\infty a_m D^{b_m} N_{os} D^{\mu_s} e^{-\lambda_s D} dD = \frac{a_m N_{os} \Gamma(1+\mu_s+b_m)}{\lambda_s^{1+\mu_s+b_m}} \tag{4}$$

Bulk water microphysics schemes are categorized in terms of the number of predicted moments, or M_n, of the size distribution. The moment of a size distribution is a statistical property, the integrated product of the diameter raised to the power n and the number concentration of the same diameter. In terms of the gamma size distribution, the n^{th} moment is defined as:

$$M_n = \frac{N_{os} \Gamma(1+\mu_s+n)}{\lambda^{1+\mu_s+n}} \tag{5}$$

Following this terminology, a single-moment microphysics scheme predicts one moment, the mass content (or M_{b_m}) of

Corresponding author: Andrew L. Molthan, NASA Marshall Space Flight Center, Huntsville, Alabama. E-mail: andrew.molthan@nasa.gov.

the particle size distribution for each precipitating species. By predicting the total mass through simulated microphysics processes, remaining terms can be determined by assigning fixed values or functions to restrict remaining parameters. As an example, an assignment of N_{os} and M(D) allow for the calculation of λ_s based upon the predicted snow mass content $(\rho_a q_s)$ acquired from simulated microphysical processes:

$$\lambda_s = \left(\frac{a_m N_{os} \Gamma(1+\mu_s+b_m)}{\rho_a q_s} \right)^{\frac{1}{1+\mu_s+b_m}} \quad (6)$$

3. The 22 January 2007 Snowfall Event and Available C3VP Data Sets

Moderate to heavy snowfall occurred over southern Ontario in advance of a warm frontal boundary, associated with a midlatitude cyclone that traveled along the U.S.-Canadian border on 22 January 2007. Precipitation began at the CARE site around 0200 UTC and continued through 0800 UTC, with the bulk of the precipitation occurring between 0600 and 0800 UTC, and a liquid equivalent total of 2.8 mm. Surface temperatures during the same period hovered near -9°C. The broad shield of warm frontal cloud cover and precipitation was sampled by the CloudSat radar, an instrumented Convair-580 aircraft, and the operational, C-band, dual-polarimetric radar at King City, Ontario. The Convair-580 was equipped to measure temperature, relative humidity, hydrometeor content with a counterflow virtual impactor (CVI, Twohy et al. 1997), and particle size distributions (PSDs) via Particle Measuring Systems (PMS) 2D-P and 2D-C probes.

In order to evaluate forecast model performance, use of aircraft data herein focuses on two portions of the flight track that represent complete vertical profiles: a descending, non-Lagrangian spiral obtained near the site of the King City radar, and the ascending departure on a southeast heading (Fig. 1). Imagery from the 2D-P and 2D-C probes were used to construct PSDs at five second increments of flight time with methods applied to avoid the adverse effects of small particles resulting from the shattering of large crystals on the probe housings (Heymsfield et al. 2008). The first and second moments were used to estimate the intercept and slope of exponential size distributions fit to each PSD (Heymsfield et al. 2004). Each PSD is accompanied by a measurement of ice water content provided by the CVI. By distributing the CVI estimate of total ice mass among the equivalent diameter spheres within the PSD, an estimate of the effective bulk density (Heymsfield et al. 2004) can be obtained and compared against forecast model assumptions.

4. Generation of WRF Model Forecasts

Comparisons between model performance and field campaign measurements require a plausible forecast of the event. Shi et al. (2010) reproduced the characteristics of the event using a triply nested, 9-3-1 km WRF model domain configuration, which was used by Molthan et al. (2010) to evaluate the assumptions of the NASA Goddard six-class, single-moment, bulk water microphysics scheme. Here, the configuration of Molthan et al. (2010) (Table 1)

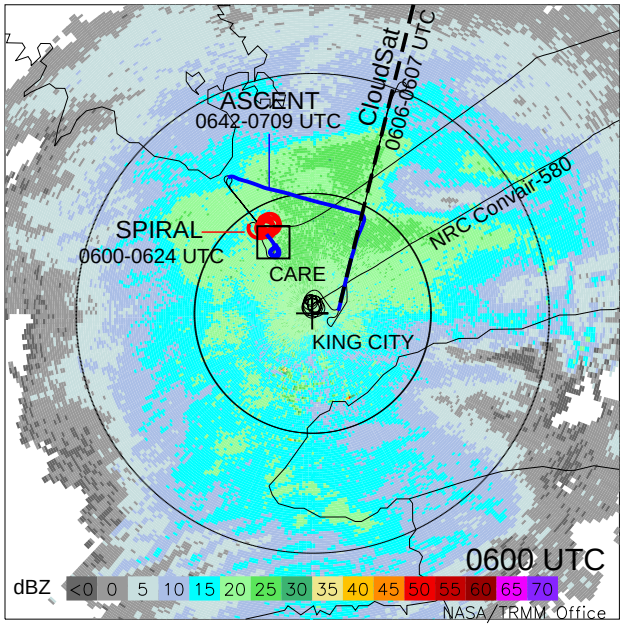

Fig. 1. Overview of some observational datasets used herein and available during the C3VP campaign. Aircraft profiles used in this study are color-coded to represent the descending spiral (red) and ascending departure (blue), and repeated in subsequent figures. The crosshair represents the location of the dual-polarimetric, C-band radar at King City, Ontario, with range rings at 50 km intervals. The dashed line to the northwest represents radar cross-sections obtained at the 331° azimuth in the direction of the CARE site.

was used to generate several additional forecasts of the 22 January 2007 event, modifying the original configuration to permit experiments using a variety of single- and double-moment schemes available within the Advanced Research (ARW) version of the WRF model version 3.1.1, and a new single-moment scheme proposed by Lin and Colle (2010). In total, six forecasts were generated to evaluate each scheme's ability to reproduce aircraft measurements of temperature, relative humidity, and properties of ice crystal size distributions, in addition to radar reflectivity and liquid equivalent precipitation.

a. Microphysics Schemes Used to Simulate the Event

The schemes used in this study offer a variety of methods to determine values of λ_s, N_{os}, mass-diameter, and diameter-fall speed relationships. Six schemes were investigated, including both single and double moment predictions, and some characteristics of each are described here. The reader is strongly encouraged to review the cited references for additional information beyond the size distribution parameterizations described here. The Goddard six-class with graupel (GSFC6G hereafter) scheme adopts the methodology of Lin et al. (1983), assigning a fixed value for N_{os} and a spherical shape representation where the effective bulk density of snow crystal populations is fixed. The WRF six-class, single-moment (WSM6) and the WRF six-class, double-moment (WDM6) schemes assume a spherical shape for snow crystals and a fixed, effective bulk density is used to define M(D), but the distribution intercept N_{os} is determined as a function

Table 1. Configuration of the WRF model for simulation of the 22 January 2007 snowfall event, following Shi et al. (2010) and Molthan et al. (2010).

Physical Process	Parameterization Scheme	Notes
Boundary Layer	Mellor-Yamada-Janjic	Janjić (1990, 1996, 2002)
Longwave Radiation	Rapid Radiative Transfer	Mlawer et al. (1997)
Shortwave Radiation	Dudhia Scheme	Dudhia (1989)
Land Surface Processes	NOAH Land Surface Model	Ek et al. (2003)
9 km Cumulus Parameterization	Grell-Devenyi Scheme	Grell and Devenyi (2002)
3,1 km Microphysics Parameterization	Varied	See text

of temperature following Houze et al. (1979). The WDM6 is equivalent to the WSM6 except that the rain category is predicted with two moments representing the total mass and number concentration. The Stony Brook University scheme (SBU-Lin, Lin and Colle 2010) uses a temperature dependent relationship for N_{os} based upon Houze et al. (1979), and a diagnosed riming factor (R_i) to estimate parameters for the mass-diameter and diameter-fall speed relationships (Lin et al. 2010). The Thompson scheme differs from other single-moment schemes by assuming a size distribution combining exponential and gamma shapes, a non-spherical mass-diameter relationship, and temperature-dependent relationships between M_2 and other M_n acquired from aircraft field campaign measurements (Field and Heymsfield 2003; Thompson et al. 2008).

Double-moment schemes predict an additional moment and provide information to better define the size distribution parameters of N_{os} and λ_s. In the Morrison scheme, the only scheme evaluated in this study that includes a double-moment representation of ice, both the mass and number concentration are predicted, based upon gamma size distributions for each hydrometeor class. Among these schemes, the Goddard, WSM6, WDM6, and Thompson schemes include prediction of the graupel class. The SBU-Lin scheme does not include a separate graupel class but incorporates variable characteristics of snow crystals dependent upon their degree of riming. The Morrison scheme does not include the prediction of graupel. Prediction of graupel is a substantial difference among the schemes presented here since the additional class would provide a variety of sources and sinks related to the production of an entirely separate category, however, observations for the 22 January 2007 event suggest that snow crystals and aggregates were the overwhelming particle type (Petersen et al. 2007), and that the simulation of graupel is not key to reproducing the character of the event. Selected characteristics of each scheme and their relevant parameters are listed in Table 2 and Table 3, respectively.

5. Surface Temperature and Precipitation

Throughout the forecast period, each of the single- or double-moment microphysics schemes produced a unique prediction of storm total precipitation related to their intrinsic assumptions and simulated processes (Fig. 2). Results herein focus on comparisons between model outputs and C3VP campaign data to determine which schemes best characterize ice crystals and aggregates for this specific event. Assessments of the relative strengths and weaknesses of each scheme would require a simliar analysis over multiple events, and a validation campaign encompassing other geographic regions and types of events.

Comparisons between CARE site air temperatures and the two meter temperatures from the nearest grid point of each forecast are shown in Fig. 3a. Modeled surface temperatures were initialized with an apparent warm bias obtained from GFS initial conditions, transitioned to a slight cool bias beginning around 1800 UTC on 21 January, and then closely followed surface temperatures through 0800 UTC on 22 January. Differences in surface temperatures between forecasts were relatively small and less than 1°C.

Individual model forecasts exhibit larger differences when examining accumulated, liquid-equivalent precipitation (Fig. 3b), compared against observed precipitation that began around 0200 UTC on 22 January. The Goddard forecast was the first to produce light precipitation at the CARE site, preceding observed accumulations by approximately four hours, while the WSM6, WDM6, Thompson, and SBU-Lin schemes lagged the observed precipitation onset by one to two hours. Since the double-moment version (WDM6) of the WSM6 retains the ice processes of the WSM6 and only provides a double moment representation for rain, accumulated precipitation in the two forecasts are equivalent with no apparent impact from any upstream processes related to the rain category. All simulations follow the general trend in precipitation accumulation, but result in an underestimate of storm total accumulation through 0800 UTC when precipitation ended at the CARE site. All forecasts continued to accumulate precipitation beyond the observed ending time. The Morrison scheme, which includes double-moment representation of all precipitating species, obtained the minimum difference between simulated and accumulated precipitation ending at 0800 UTC and performed best overall when predicting hourly and storm total accumulations.

6. Hydrometeor Profiles

In a simulation of the 22 January 2007 event by Shi et al. (2010), the model forecast was deemed able to reproduce the general onset and character of precipitation. Molthan et al. (2010) demonstrated comparable precipitation coverage between the Goddard scheme forecast and radar observations at 0600 UTC, justifying comparisons between aircraft data and model profiles within 50 km of the King City radar. Here, the 50 km range of profiles is replicated, with conditional mean profiles of non-zero hydrometeor content shown in Fig. 4. Although these schemes produce up to six hydrometeor categories and their total ice contents are comparable to aircraft estimates available through CVI measurements,

Table 2. Characteristics of Microphysics Schemes Used in Generating WRF Model Forecasts

Scheme	Moments	Notes	Selected References
Goddard	1	Saturation adjustment by Tao and Simpson (1993)	Tao et al. (2003)
WSM6	1	$N_{os}(T)$ by Houze et al. (1979)	Hong et al. (2004)
SBU-Lin	1	$N_{os}(T)$ by Houze et al. (1979)	Lin and Colle (2010)
		M(D) functions of diagnosed riming factor R_i, T	Lin et al. (2010)
		V(D) functions of diagnosed riming factor R_i, T	
Thompson	1	Predicts M_n as $f(M_2, T)$ from Field et al. (2005)	Thompson et al. (2008)
		$V(D) = a_v D^{b_v} e^{-f_v}$, $f_v = 125$	
WDM6	2	Double moment only applies to rain category	Hong et al. (2010)
Morrison	2	Number concentration and mass for each species	Morrison et al. (2005)

Table 3. Parameters Defining Relationships Within Microphysics Schemes Used in Generating WRF Model Forecasts

Scheme	N_{os} (m^{-4})	μ_s	ρ_s $(kg\ m^{-3})$	a_m $(kg\ m^{-b_m})$	b_m	λ_s (m^{-1})	a_v $(m^{1-b_v}\ s^{-1})$	b_v
Goddard	1.6×10^7	0	100	$\frac{\pi}{6}\rho_s$	3.0	(6)	1.305	0.11
WSM6	$f(T)$	0	100	$\frac{\pi}{6}\rho_s$	3.0	(6)	11.72	0.41
SBU-Lin	$f(T)$	0	$f(D)$	$f(T,R_i)$	$f(T,R_i)$	(6)	$f(T,R_i)$	$f(T,R_i)$
Thompson	N/A	N/A	$f(D)$	0.069	2.0	N/A	40.0	0.55
WDM6	$f(T)$	0	100	$\frac{\pi}{6}\rho_s$	3.0	(6)	11.72	0.41
Morrison	$f(M_0,\lambda_s)$	0	100	$\frac{\pi}{6}\rho_s$	3.0	(6)	11.72	0.41

each partitions the total ice content in different ways based upon their varied assumptions and simulated processes. None of the forecasts produced an appreciable amount of graupel, in agreement with digital photographs of large, lightly rimed aggregates that occurred at the surface (Petersen et al. 2007). The Goddard scheme was the only forecast to produce an appreciable profile of cloud liquid water content, although no significant amounts of liquid water were detected by aircraft instrumentation. This is likely a result of the order of microphysics operations within the code and discussed within Molthan et al. (2010).

Each of the forecasts differ substantially in their partitioning of total ice mass among the cloud ice and snow categories. In each forecast, cloud ice contributes to the eventual development of snow mass through autoconversion, accretion, and deposition. Differences in the handling of these processes lead to varied profiles of cloud ice and snow mass. Precipitation in the Goddard scheme is characterized by an upper level (4-6 km) layer of cloud ice which transitions to the snow category around 4 km. The SBU-Lin and Morrison forecasts also produced a layer of cloud ice from 4-6 km, but with a reduced mass content and a faster transition to the snow category. In the Thompson forecast, the vertical profile is dominated by the snow category. In the WSM6 and WDM6 formulation, the cloud ice profile exceeds the snow category at altitudes of 1 km and above, representing precipitation as large number concentrations of pristine ice crystals rather than aggregates.

7. Temperature and Water Vapor Profiles

In addition to the solid or liquid species, each scheme handles the sources and sinks of water vapor through phase change processes, contributing to sources or sinks for the hydrometeor classes, and latent heating within the vertical profile. Mean temperature profiles were constructed for each scheme using the same sets of model vertical profiles obtained within 50 km of the King City radar installation. Absolute differences between the mean temperature profiles for each forecast were less than 0.5°, with the largest differences focused in the lowest 1-2 km of the vertical profile, and all forecasts exhibiting a slight warm bias in the entire vertical column (Fig. 5).

In order to compare simulated water vapor profiles against aircraft data, water vapor fields were converted to relative humidities with respect to water and ice and reported as the maximum value at each model vertical level. Greater differences in relative humidity occur, given the variety of mechanisms for initiating precipitation within each scheme, and their respective methods for implementing saturation adjustments. Aircraft data indicate that the entire vertical column was saturated (supersaturated) with respect to water (ice), but each scheme obtains various levels of saturation depending upon their assumptions and parameterizations (Fig. 6). Molthan et al. (2010) noted the discrepancy in saturation levels that occurs within the Goddard scheme forecast at temperatures colder than -15°C, attributed to a temperature threshold within the Tao and Simpson (1993) saturation adjustment scheme, an assumption repeated here. The WSM6 and WDM6 forecasts are not saturated (subsaturated) with respect to water (ice), related to their handling of depositional growth or saturation adjustment processes. The SBU-Lin forecast allows for a linear decrease in supersaturation with respect to ice between 500 and 300 hPa. Although the SBU-Lin forecast approaches saturation with respect to water in the lowest 1-2 km, values decrease with decreasing pressure. The Thompson and Morrison schemes produce the best

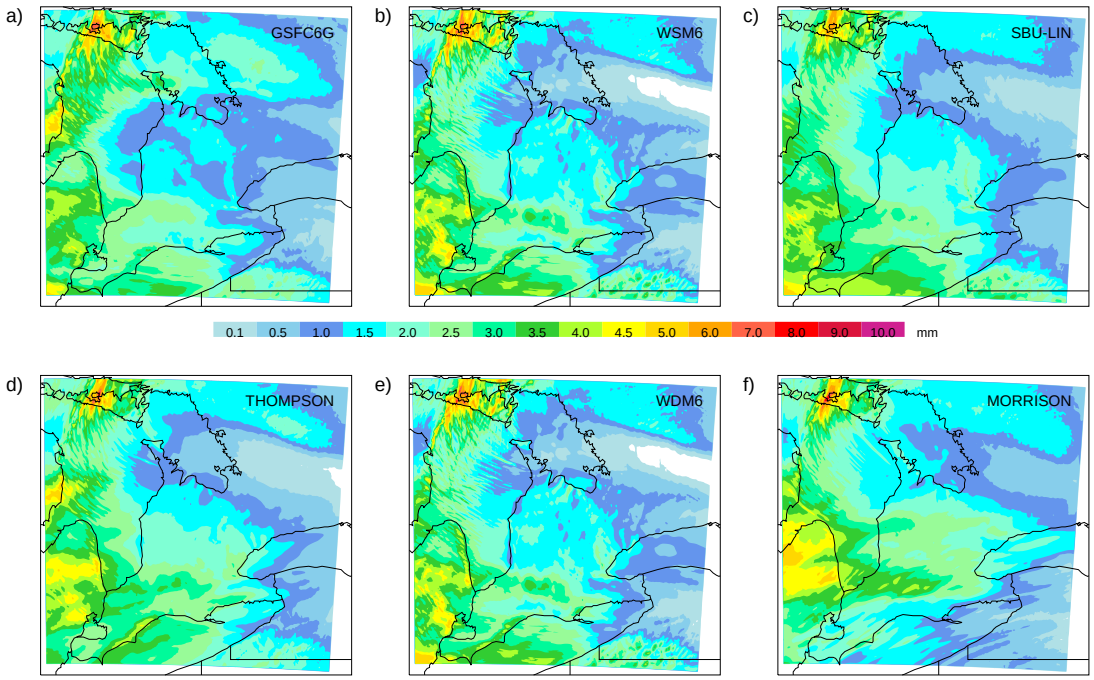

Fig. 2. Storm total, liquid equivalent precipitation through 0600 UTC on 22 January 2007 for each of simulations employed in this study.

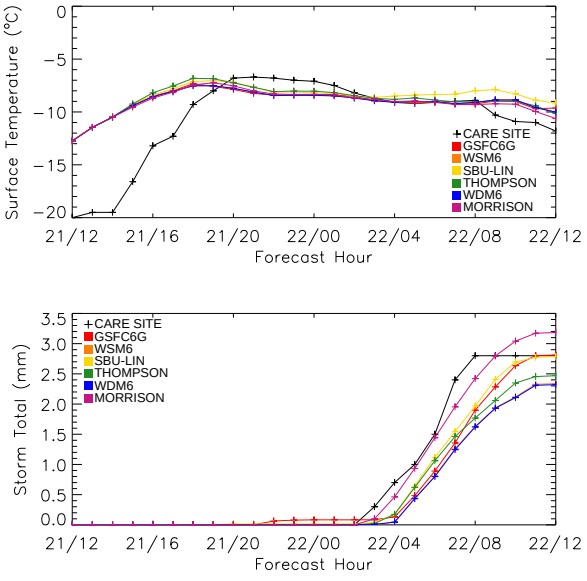

Fig. 3. Comparisons of observed and predicted 2 m air temperatures at the CARE site (top) and storm total, liquid equivalent precipitation accumulation, based upon six WRF forecasts of the 22 January 2007 snowfall event.

representation of the water vapor profile, each maintaining values near saturation with respect to water except for a minor reduction near 4 km.

8. Size Distribution Parameters

Five of the six aforementioned schemes assign an exponential size distribution to precipitating hydrometeors, a special case of the gamma distribution (1) where the dispersion parameter μ_s is set to zero. Aircraft estimates of N_{os} and λ_s were acquired from C3VP aircraft profiles shown in Fig. 1, retaining parameters that provide a reliable fit ($R^2 \geq 0.8$) between the resulting exponential distribution and the actual PSD. Aircraft estimates of size distribution parameters can be compared against model assumptions or outputs for all forecasts except the Thompson scheme. Discussions related to the Thompson scheme are deferred to the next section where the performance of each scheme is examined in terms of distribution moments.

Mean profiles of particle size distribution parameters were acquired from WRF model vertical profiles within 50 km of the King City radar, then compared against aircraft measurements (Fig. 7). The constant value of N_{os} in the Goddard forecast was incapable of representing vertical variability in aircraft observations (Molthan et al. 2010). The WSM6, WDM6 and SBU-Lin schemes determine N_{os} using Houze et al. (1979) function of temperature and provide for some variability in N_{os} and λ_s with height, except for the lowest 1-2 km of the vertical profile where temperatures are nearly isothermal. Values of a_m and b_m within the SBU-Lin scheme are determined from local calculation of the riming factor R_i (Lin and Colle 2010). These calculations of a_m and b_m are less than the $\frac{\pi}{6}\rho_s$ used within the WSM6 and WDM6 and permit a reduction in λ_s despite an increase in the simulated,

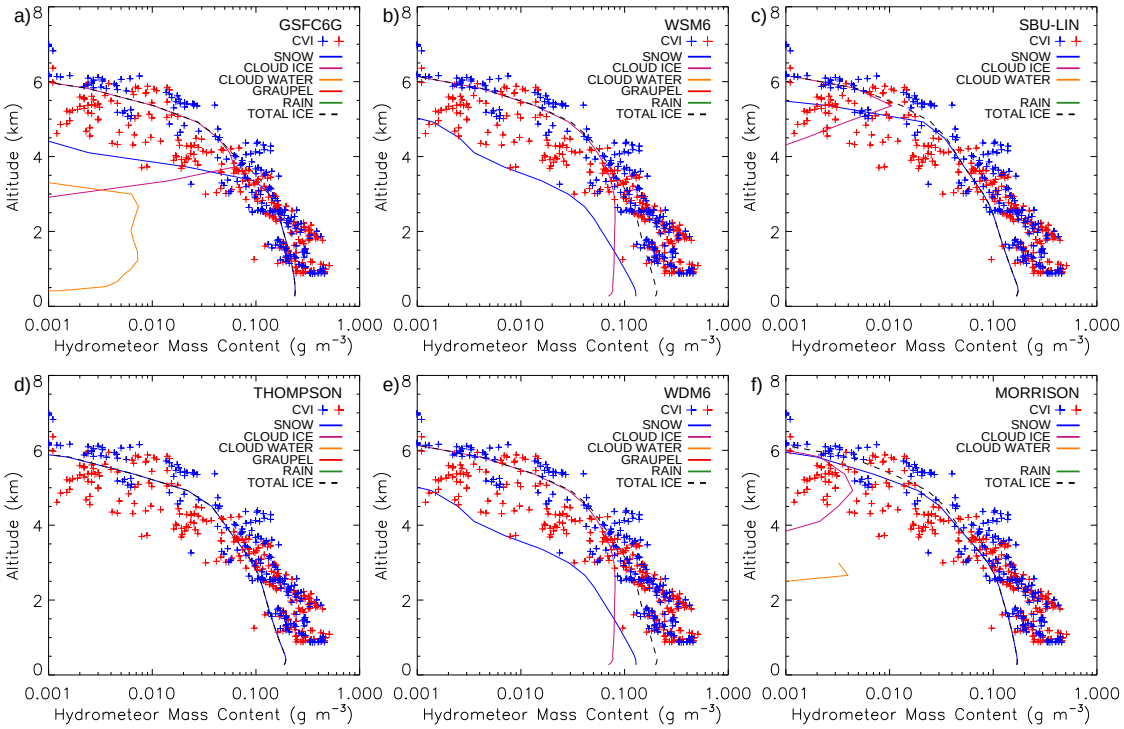

Fig. 4. Profiles of hydrometeor content obtained as conditional means from WRF model grid points within 50 km of the King City radar location, compared with observations of ice water content provided by the CVI instrument aboard the Convair-580 aircraft. Total ice profiles represent the sum of cloud ice, snow, and graupel categories, where available. Color coding of aircraft data represents the profiles described in Fig. 1.

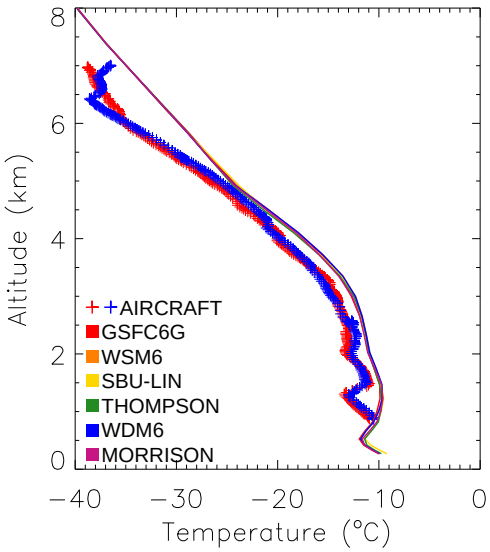

Fig. 5. Mean profiles of air temperature from WRF model grid points within 50 km of the King City radar location, compared with observations acquired fromthe Convair-580 aircraft data.

snow mass content (Fig. 4).

9. Moments of Particle Size Distributions

The Thompson scheme is unique because it uses microphysical processes to acquire ice mass (M_2) and then uses equations relating M_2 and temperature to calculate other moments needed in the simulation of microphysical processes. Other schemes use the exponential size distribution and parameters to determine remaining moments needed to simulate processes and rely upon either fixed values or temperature-dependent functions to characterize N_{os}. Given the disparity in techniques used to characterize PSDs within the aforementioned schemes, comparisons are made using mean profiles of various M_n from WRF model profiles within 50 km of the King City radar (Fig. 8). Analysis focuses on contributions from the snow mass category. Except for the Morrison scheme, remaining schemes assume a monodisperse assignment for the cloud ice class. Determinination of the size or number concentration of cloud ice crystals varies within each scheme but large number concentrations of very small particles were not found to contribute significantly to moments of order greater than M_0.

Comparisons of M_0 represent the ability to represent the total number concentration (Fig. 8a). Observations suggest that total number concentrations decrease between cloud top and cloud base as larger aggregates develop from mergers of smaller crystals, reducing the total number of particles. This coincides with increases in total ice water content through deposition and light riming. The Morrison scheme replicates the general trend in M_0 decrease toward cloud

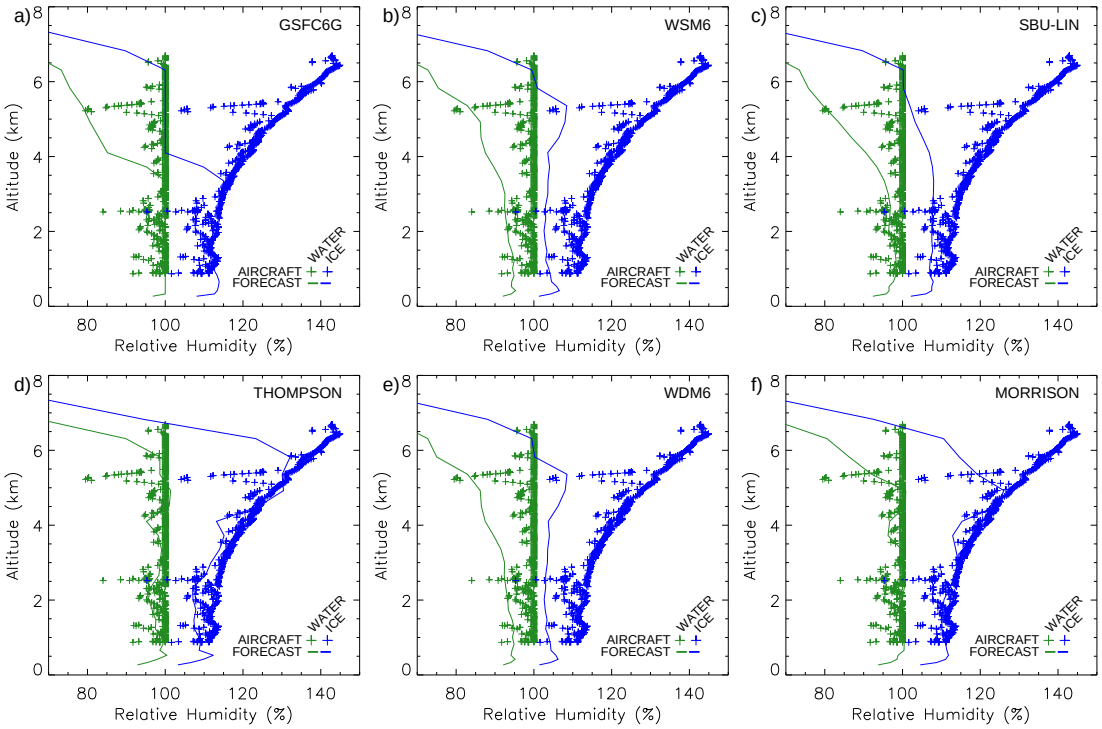

Fig. 6. Mean profiles of relative humidities with respect to water and ice from WRF model grid points within 50 km of the King City radar location, compared with observations acquired from the Convair-580 aircraft data.

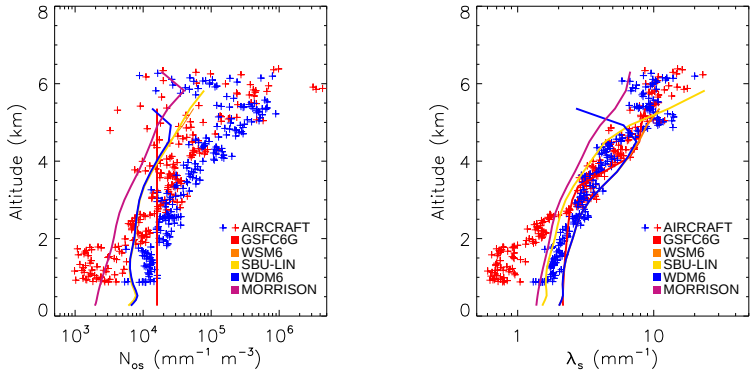

Fig. 7. Mean vertical profiles of N_{os} and λ_s acquired from WRF model grid points within 50 km of the King City radar, based upon assumptions and predicted snow contents unique to each scheme. Model results are compared against PSDs and their parameter estimates, acquired from aircraft profiles shown in Fig. 1.

base, likely benefitting from the double-moment representation of both mass and total number concentration. The Thompson scheme forecast overestimated observed values of M_0 and failed to represent the trend of increasing M_0 with decreasing height, despite functional relationships of temperature and predicted M_2 that provide flexibility in size distribution assignment. Remaining single-moment schemes employ a variety of strategies for determining M_0. Since each scheme uses an exponential size distribution, M_0 is the ratio between the distribution intercept and slope parameter. The SBU-Lin, WSM6 and WDM6 forecasts use the Houze et al. (1979) relationship for $N_{os}(T)$, and although they underestimate observations, they follow the general increase in observed N_{os} with height (Fig. 7). As the lapse rate of temperature is reduced in the lowest 3 km (Fig. 5), variablity in similated N_{os} decreases, while observed values continue to decrease due to aggregation. The λ_s parameter is calculated based upon the snow content and assignment of N_{os} (6), with underestimates (overestimates) of N_{os} contributing to underestimates (overestimates) of λ_s and particle size distributions with mean crystal sizes larger (smaller) than suggested by aircraft PSDs. The Goddard forecast produced

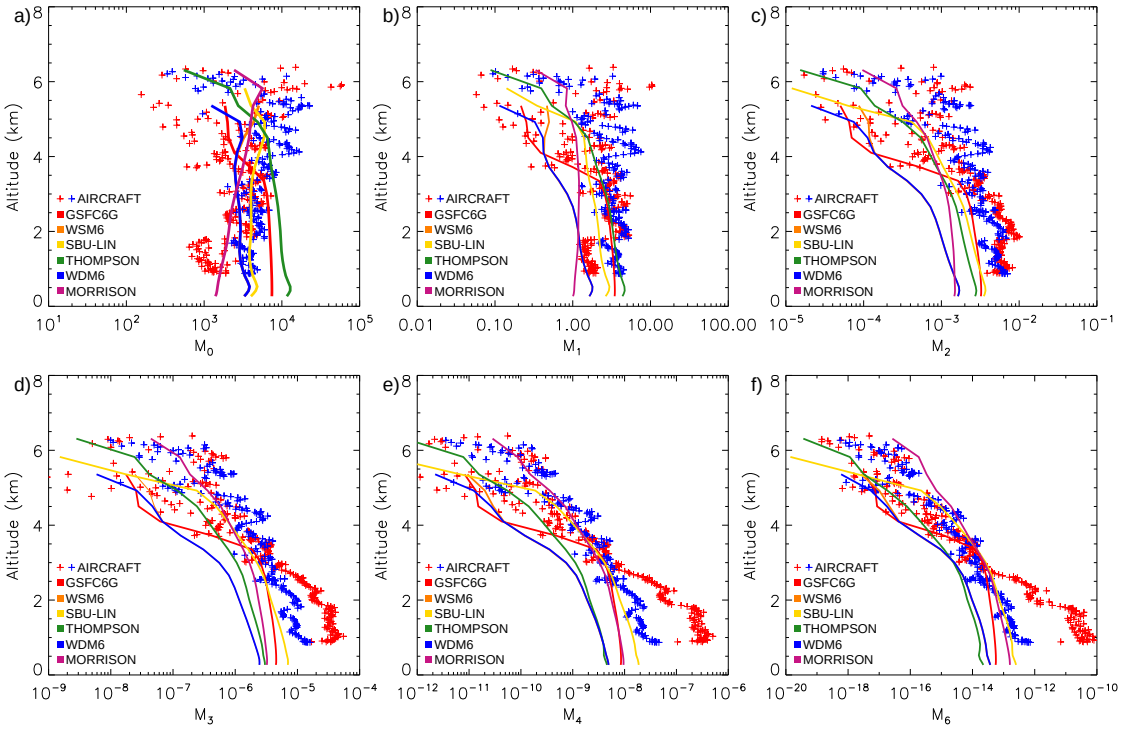

Fig. 8. Mean profiles of various moments of simulated particle size distributions for the snow category, based upon varying scheme assumptions, compared against moments derived from aircraft measured particle size distributions acquired in 5 s intervals. Color coding of aircraft data represents the profiles described in Fig. 1.

little variability in M_0 within the lowest 4 km, attributable to the use of a constant size distribution intercept and snow bulk density.

Determination of M_2 is crucial for the Thompson scheme. Within the Thompson scheme, prediction of the total ice water content is related to M_2 through the assignment of the mass-diameter relationship, and M_2 is used to calculate additional moments, with M_n as functions of M_2 and temperature. This avoids the use of constants within the prescribed size distribution and allows for vertical variability observed in nature as a function of M_2 and temperature (Field et al. 2005). In this particular event, the Thompson scheme underestimated M_2, particularly in the lowest 3 km, where large aggregates were observed (Molthan et al. 2010). Due to the underestimate of M_2 and the limited range in temperature within the observed and simulated profiles (Fig. 8c), predicted, higher order moments continued to underestimate aircraft observations. Attempts by the Thompson scheme to use M_2 and temperature to predict other moments have merit, as mean profiles of M_{1-6} replicate the general trend in vertical variabilty. However, it may be that the rapid onset of aggregation in this specific event is not well represented by the Field et al. (2005) relationships of $f(M_2, T)$ currently used within the scheme. Modification of the $f(M_2, T)$ relationships to better fit this event may improve upon the current fit between aircraft and simulated PSD moments.

Other moments shown in Fig. 8 demonstrate observed vertical trends and the ability of each scheme to replicate other characteristics of aircraft particle size distributions. Depending upon the assignment of PSD characteristics, successful representation of lower order moments do not guarantee successful estimate of higher order moments, since higher order moments are increasingly sensitive to weighting by relatively small number concentrations of large targets (5). For example, although mean profiles of M_1 acquired from the Morrison scheme underestimate aircraft observed values, this underestimation is reduced for higher order moments of M_2 through M_3, and the scheme produces mean profiles of M_4 and M_6 that provide a good representation of values within the ascending aircraft profile. In a single-moment representation, the SBU-Lin forecast slightly underestimated M_2 values throughout the bulk of the profile, but produced a reasonable depiction of M_4 and M_6, providing a better fit to aircraft observations than the two-moment representation of the Morrison scheme. Profiles of λ_s and N_{os} for the SBU-Lin scheme indicate that both parameters are generally underestimated, but higher order moments are inversely proportional to λ_s^{1+n} (5), so that underestimates (overestimates) of λ_s (mean particle size) contribute to larger, predicted values of $M_{4,6}$. Simulated decreases in λ_s and N_{os} between cloud top and cloud base represent an ability to represent some of the effects of aggregation within the single-moment formulation, comparable to the Morrison double-moment representation. The Thompson scheme is capable of representing the vertical trend in $M_{4,6}$ but would need some modification to internal functions of M_2 and temperature in

order to increase predicted values of $M_{4,6}$. For comparison, the WSM6 and WDM6 forecasts predict values of λ_s and N_{os} that are too large, or a total particle number concentration and mean aggregate diameter less than observed, resulting in a substantial underestimate of $M_{4,6}$. Mean profiles from the Goddard scheme struggle to represent the vertical variability observed in aircraft data due to strict adherence to constants, described previously by Molthan et al. (2010).

10. Comparisons of Radar Reflectivity Profiles

Radar reflectivity is often used as a post-processed model variable becuase it quickly depicts the coverage, structure, and relative intensity of precipitation within the forecast domain. The methodology of Smith (1984) was used to convert predicted ice water content and size distribution to a simulated reflectivity value based upon diameters of equivalent mass, pure ice spheres. The resulting equation for an equivalent radar reflectivity factor (Z_e) from forecast model output is:

$$Z_e = \frac{|K|_i^2}{|K|_w^2} Z, \tag{7}$$

where the coefficient represents the ratio of the dielectric factors for ice and water, multiplied by the radar reflectivity factor Z, acquired from spheres with ice mass equivalent to simulated snow crystals. By including all possible variability in particle size distribution and mass-diameter relationships, Z can be obtained from forecast model output as:

$$Z = \left(\frac{6a}{\pi\rho_i}\right)^2 \int_0^\infty D^{2b} D^\mu N(D) dD. \tag{8}$$

The Goddard, WSM6, WDM6, and Morrison schemes represent snow crystals as spherical shapes within an exponential size distribution and with a fixed bulk density, so that $a_m = \frac{\pi}{6}\rho_s$, $b_m = 3$, and $\mu = 0$ (Table 3). This combination of variables results in Z proportional to M_6, and resulting reflectivity profiles will be comparable to the M_6 vertical profile. The Thompson scheme uses a fixed a_m and $b_m = 2$, resulting in similarity to M_4. Since the SBU-Lin forecast provides for flexibility in both a_m and b_m, moments used in the calculation of Z will vary between M_4 and M_6.

In order to evaluate model performance, the 0600 UTC volume scan of King City horizontally polarized radar reflectivity is compared against values simulated from model output, based upon vertical profiles within 50 km of the radar location. Observed radar reflectivity was used to construct a contoured frequency with altitude diagram (CFAD, Yuter and Houze 1995) with histogram increments of 2 dBZ and 500 m (Fig. 9). The mean profile of simulated reflectivity provides a comparison between modeled values and the relative frequency of observations within the same altitude range. Differences in modeled and simulated reflectivity relate to the size distribution, mass-diameter relationship, and snow mass content for each scheme.

Since the Thompson and SBU-Lin schemes use information from the ambient environment to allow for variability in PSD and M(D) relationships within the vertical, their mean profiles represent the general, vertical trend in modal reflectivity values shown within the King City CFAD. The WSM6/WDM6 schemes incorporate a temperature-dependent particle size distribution and follow the vertical trend in radar reflectivity below 2 km, but the rapid transition from snow to cloud ice content contributes to a sharper decrease in radar reflectivity with altitude than observed by the King City radar.

In this case, single-moment schemes incorporating vertical variability in snow characteristics are capable of representing the vertical trend in King City radar reflectivity, but the Thompson and SBU-Lin schemes provide a better fit by maintaining populations of large, precpitating ice crystals through a deeper portion of the vertical column. Although the Goddard scheme provides the best fit between CVI estimates of IWC and predicted snow mass, fixed values of ρ_s and N_{os} result in a reduced reflectivity lapse rate and a median profile that does not represent observed trends in the lowest 3 km. Above the 3 km level, the rapid transition between snow and cloud ice reduces the median reflectivity profile in a manner similar to the WSM6/WDM6 forecasts.

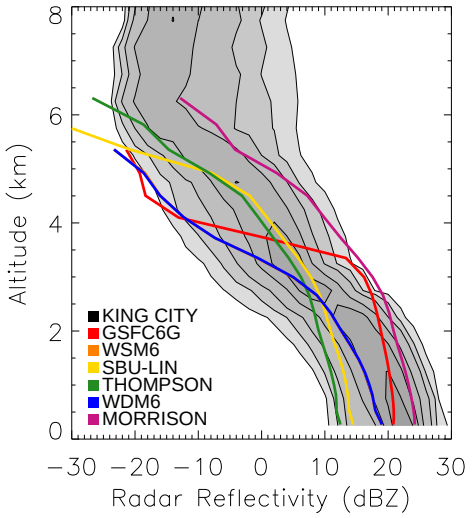

Fig. 9. Mean vertical profiles of N_{os} and λ_s acquired from WRF model grid points within 50 km of the King City radar, based upon assumptions and predicted snow contents unique to each scheme. Model results are compared against PSDs and their parameter estimates, acquired from aircraft profiles shown in Fig. 1.

11. Comparisons of Terminal Fall Speed Relationships

Terminal fall speeds of snow crystals were measured at the CARE site using a Hydrometeor Velocity and Shape Detector (HVSD, Barthazy et al. 2004), which images crystals passing between a series of digital detectors, and uses repeated imagers to estimate fall speeds. Resulting crystal fall speeds were provided by GyuWon Lee (McGill University) after determining that wind did not bias fall speeds during the snowfall period. It is assumed herein that the reported fall velocities are the terminal velocities for each crystal.

Observations of fall speed were binned for each HVSD maximum dimension bin diameter at 5 cm s^{-1} increments, accumulated for over 11,000 individual flakes observed from 0200 to 0800 UTC (Fig. 10). Sizes and terminal velocities were fit to the power law form of Locatelli and Hobbs (1974), but were restricted to sizes greater than 1 mm and with at least 50 observations to account for limitations in HVSD detection of small particles and provide for a reasonable sample size.

The best fit relationship for HVSD crystals produced values of $a_v = 110.083$ cm^{1-b_v} s^{-1} and $b_v = 0.145$, comparable to Locatelli and Hobbs (1974) values for "unrimed radiating assemblages of dendries" ($a_v = 80.0$ cm^{1-b_v} s^{-1}, b_v=0.16). Molthan et al. (2010) attributed this similarity to the presence of large aggregates dominating the lowest levels of aircraft and dual-polarimetric radar observations. Simulated hydrometeor mass flux and resulting precipitation are sensitive to both the particle size distribution and the chosen relationship between diameter and fall speed.

Comparisons between the HVSD best-fit relationship and each forecast scheme (Table 3) are shown in Fig. 10. The Goddard forecast underestimates fall speeds at all diameters, while the Morrison and WSM6/WDM6 forecasts overestimate (underestimate) fall speeds for particles larger than 2 mm (smaller than 1 mm). The SBU-Lin scheme is the best fit to observations, although a slight overestimate occurs for all fall speeds, on the order of 0.1 m s^{-1}. The Thompson scheme oversetimates fall speeds for particles larger than 1 mm, but includes an expoential decay term to reduce the fall speeds of large particles. Although the adjustment was not strong enough for this case, it is an improvement over the Morrison, WSM6, and WDM6 schemes where the overestimate continues to grow with increase in particle maximum dimension. Although the Morrison scheme produced the best fit to observed surface precipitation accumulation (Fig. 3) and the simulation of aggregation benefits from the inclusion of the second moment (Fig. 7), the higher precipitation rate may have been obtained by overestimating particle fall speeds. Conversely, the SBU-Lin scheme provided the best overall fit to particle fall speeds, but prediced snow content was less than the mass acquired from CVI measurements (Fig. 4), and simulated particle size distributions may have produced a mean size larger than observations, combining for a precipitation rate closer to observations. Conclusions about model performance based upon sensible weather elements such as precipitation rate should also consider the reliability of assumptions in particle size distribution, mass-diameter relationship, and fall speeds.

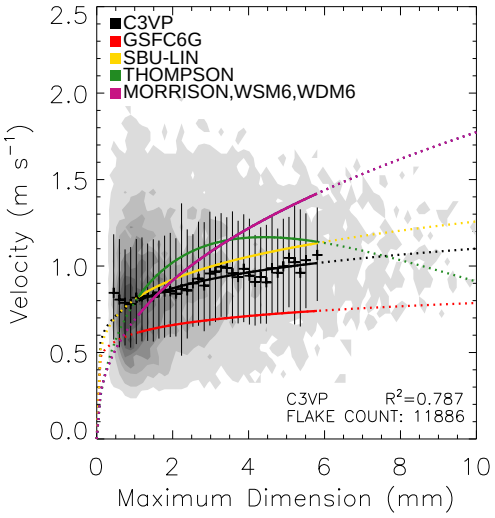

Fig. 10. Mean vertical profiles of N_{os} and λ_s acquired from WRF model grid points within 50 km of the King City radar, based upon assumptions and predicted snow contents unique to each scheme. Model results are compared against PSDs and their parameter estimates, acquired from aircraft profiles shown in Fig. 1.

12. Summary and Conclusions

An intensive observation period of the C3VP field campaign measured snow crystal particle size distributions, ice water content, and other atmospheric state variables within a broad region of snowfall associated with a passing midlatitude cyclone on 22 January 2007. Simulations of the event were performed with the Advanced Research WRF version 3.1.1, using a baseline set of physical parameterizations with various selections of single and double-moment microphysics schemes. The resulting model output fields of hydrometeor content, water vapor, and temperature were compared to *in situ* aircraft and surface measurements. Assumptions of particle size distribution, mass-diameter relationship, and diameter-terminal velocity relationships were evaluated using available C3VP datasets.

Each of the single and double-moment schemes have various strengths and weaknesses, but all produced a reasonable simulation of the event, including surface temperatures and liquid equivalent precipitation rates. The representation of diverse size distrbutions and particle effective bulk densities is best schieved by incorporating variability in size distribution parameters and mass-diameter relationships. These strategies are employed by the WSM6/WDM6, the Thompson, and the SBU-Lin forecasts which use a temperature-dependent size distribution intercept, temperature-dependent relationships between various size distribution moments, or the local prediction of size distribution, fall speed, and density characteristics as a function of crystal riming. Fixed values for these characteristics are often unable to represent changes in crystal characteristics throughout the vertical column. Double-moment representation in the Morrison scheme assists in the depiction of the aggregation process by allowing for better representation of total particle number concentrations, but could be improved upon by allowing for greater flexibility in the remaining mass-diameter and fall speed relationships. It is unlikely and perhaps unrealistic to expect any given scheme to precisely simulate the characteristics of a single event, but field campaign data sets should be examined where available to evaluate the assumptions present within various physical parameterizations given their increased utilization in current operational or experimental weather forecast models.

In the interim, ensemble prediction strategies that combine various scheme outputs into a range of plausible events may assist in local, high resolution forecasts

ACKNOWLEDGMENTS

Model simulations were performed on the NASA Discover Cluster. Data from the HVSD instrument were provided by GyuWon Lee of McGill University. Prime funding for aircraft studies during the Canadian CloudSat/CALIPSO Validation Project was provided by the Canadian Space Agency. The author thanks the creators of the SBU-Lin scheme for providing a version of their scheme used in this experiment.

REFERENCES

Barthazy, E., S. Goke, R. Schefold, and D. Hogl, 2004: An optical array instrument for shape and fall velocity measurements of hydrometeors. *J. Atmos. Oceanic Technol.*, **21**, 1400–1416.

Bernardet, L., et al., 2008: The Developmental Testbed Center and its winter forecasting experiment. *Bull. Amer. Meteor. Soc.*, **89**, 611–627.

Dudhia, J., 1989: Numerical study of convection observed during the winter monsoon experiment using a mesoscale two-dimensional model. *J. Atmos. Sci.*, **46**, 3077–3107.

Ek, M., M. E. Mitchell, Y. Lin, E. Rogers, P. Grunmann, V. Koren, G. Gayno, and J. D. Tarpley, 2003: Implementation of NOAH land surface model advances in the National Centers for Environmental Prediction operational mesoscale Eta model. *J. Geophys. Res.*, **108**.

Field, P. R. and A. J. Heymsfield, 2003: Aggregation and scaling of ice crystal size distributions. *J. Atmos. Sci.*, **60**, 544–560.

Field, P. R., R. J. Hogan, P. R. A. Brown, A. J. Illingworth, T. W. Choularton, and R. J. Cotton, 2005: Parameterization of ice-particle size distributions for mid-latitude stratiform cloud. *Quart. J. Roy. Meteor. Soc.*, **131**, 1997–2017.

Grell, G. A. and D. Devenyi, 2002: A generalized approach to parameterizing convection combining ensemble and data assimilation techniques. *Geophys. Res. Lett.*, **29**, D00A09, doi:10.1029/2007JD009766.

Heymsfield, A., A. Bansemer, C. Schmitt, C. Twohy, and M. Poellot, 2004: Effective ice particle densities derived from aircraft data. *J. Atmos. Sci.*, **61**, 982–1003.

Heymsfield, A. J., P. Field, and A. Bansemer, 2008: Exponential size distributions for snow. *J. Atmos. Sci.*, **65**, 4017–4031.

Hong, S.-Y., J. Dudhia, and S.-H. Chen, 2004: A revised approach to ice microphysical processes for the bulk parameterization of clouds and precipitation. *Mon. Wea. Rev.*, **132**, 103–120.

Hong, S.-Y., K.-S. S. Lim, Y.-H. Lee, J.-C. Ha, H.-W. Kim, S.-J. Ham, and J. Dudhia, 2010: Evaluation of the WRF double-moment six-class microphysics scheme for precipitating convection. *Advances in Meteorology*, **2010**, 707 253.

Houze, R. A. J., P. V. Hobbs, P. H. Herzegh, and D. B. Parsons, 1979: Size distributions of precipitation particles in frontal clouds. *J. Atmos. Sci.*, **36**, 156–162.

Janjić, Z. I., 1990: The step-mountain coordinate: Physical package. *Mon. Wea. Rev.*, **118**, 1429–1443.

Janjić, Z. I., 1996: The surface layer in the NCEP Eta model. *Preprints, 11th Conference on Numerical Weather Prediction, American Meteorological Society*, Norfolk, VA, Amer. Meteor. Soc., 354–355.

Janjić, Z. I., 2002: Nonsingular implementation of the Mellor-Yamada level 2.5 Scheme in the NCEP Meso model. *NCEP Office Note*, 61, 437.

Kain, J. S., S. J. Weiss, J. J. Levit, M. E. Baldwin, and D. R. Bright, 2006: Subjective verification of numerical models as a component of a broader interaction between research and operations. *Wea. Forecasting*, **18**, 847–860.

Lin, Y. and B. A. Colle, 2010: A new bulk microphysical scheme that includes riming intensity and temperature dependent ice characteristics. *Mon. Wea. Rev.*, early online release.

Lin, Y., L. J. Donner, and B. A. Colle, 2010: Parameterization of riming intensity and its impact on ice fall speed using ARM data. *Mon. Wea. Rev.*, early online release.

Lin, Y.-L., R. D. Farley, and H. D. Orville, 1983: Bulk parameterization of the snow field in a cloud model. *J. Appl. Meteor.*, **22**, 1065–1092.

Locatelli, J. D. and P. V. Hobbs, 1974: Fall speeds and masses of solid precipitation particles. *J. Geophys. Res.*, **79**, 2185–2197.

Marshall, J. S. and W. M. Palmer, 1948: The distribution of raindrops with size. *Journal of the Atmospheric Sciences*, **5**, 165–166.

Mlawer, E. J., S. J. Taubman, P. D. Brown, M. J. Iacono, and S. A. Clough, 1997: Radiative transfer for inhomogeneous atmosphere: RRTM, a validated correlated-k model for the long-wave. *J. Geophys. Res.*, **102**, 16 663–16 682.

Molthan, A. L., W. A. Petersen, S. W. Nesbitt, and D. Hudak, 2010: Evaluating the snow crystal size distribution and density assumptions within a single-moment microphysics scheme. *Mon. Wea. Rev.*, **138**, 4254–4267.

Morrison, H., J. A. Curry, and V. I. Khvorostyanov, 2005: A new double-moment microphysics parameterization for application in cloud and climate models. Part I:Description. *J. Atmos. Sci.*, **62**, 1665–1677.

Petersen, W. A., et al., 2007: NASA GPM/PMM participation in the Canadian CloudSat/CALIPSO validation project C3VP: Physical process studies in snow. *Preprints, 33rd International Conference on Radar Meteorology*, 1–7, Cairns, Australia, 6-10 August 2007.

Shi, J. J., et al., 2010: WRF simulations of the January 20-22 2007 snow events over eastern Canada: Comparison with in-situ and satellite observations. *J. Appl. Meteor. Climatol.*, early Online Release.

Smith, P., 1984: Equivalent radar reflectivity factors for snow and ice particles. *Journal of Applied Meteorology*, **23**, 1258–1260.

Tao, W.-K. and J. Simpson, 1993: Goddard cumulus ensemble model. Part I: Model description. *Terrestrial Atmospheric and Oceanic Sciences*, **4**, 35–72.

Tao, W.-K., et al., 2003: Microphysics, radiation and surface processes in the Goddard Cumulus Ensemble (GCE) model. *Meteor. Atmos. Phys.*, **82**, 97–137.

Thompson, G., P. R. Field, R. M. Rasmussen, and W. D. Hall, 2008: Explicit forecasts of winter precipitation using an improved bulk microphysics scheme. Part II: Implementation of a new snow parameterization. *Mon. Wea. Rev.*, **136**, 5095–5115.

Twohy, C. H., A. J. Schanot, and W. A. Cooper, 1997: Measurement of condensed water content in liquid and ice clouds using an airborne counterflow virtual impactor. *J. Atmos. Oceanic Technol.*, **14**, 197–202.

Yuter, S. and R. Houze, 1995: Three-dimensional kinematic and microphysical evolution of Florida cumulonimbus. Part II: Frequency distributions of vertical velocity, reflectivity and differential reflectivity. *Mon. Wea. Rev.*, **123**, 1941–1963.